Experimental and model validation of a phase change material heat exchanger integrated into a real building

Received: 9 February 2021 | Revised: 6 April 2021 | Accepted: 27 April 2021

DOI: 10.1002/er.7037

SHORT COMMUNICATION

INTERNATIONAL JOURNAL OF ENERGY RESEARCH WILEY

Experimental and model validation of a phase change material heat exchanger integrated into a real building

Gabriele Triscari[1] | **Michele Santovito**[2] | **Maurizio Bressan**[1] | **Davide Papurello**[1,3]

[1]Department of Energy (DENERG), Politecnico di Torino, Turin, Italy

[2]i-TES, Thermal Energy Storage, Turin, Italy

[3]Energy Center, Politecnico di Torino, Turin, Italy

Correspondence
Davide Papurello, Department of Energy (DENERG), Politecnico di Torino, Corso Duca degli Abruzzi, 24, 10129, Turin, Italy.
Email: davide.papurello@polito.it

Summary

Latent heat thermal energy storages (LHTES) are a promising technology with a wide range of applications in the framework of energy efficiency improvement. Phase change materials provide a big storage capacity, but their thermal conductivities are always extremely low. The use of finned tube heat exchangers is nowadays the best solution to enhance PCMs thermal performances. This allows significant charging and discharging rates. The major challenge concerns the balance between thermal performances and high material costs. A proper design of the heat transfer surfaces is essential to limit the system overall cost. Two different heat exchangers solutions, with radial and longitudinal fins are here examined. The design of the LHTES is performed by deploying a simplified FEM numerical model specifically developed for the application. A validation procedure based on laboratory tests with a small LHTES prototype was also carried out. The obtained results confirmed the reliability of the numerical model and justify its adoption as a tool for the design phase. The FEM model allows to effectively simulate the system thermal behaviour and assess the impact of the different HEX geometrical parameters on thermal performances. Based on this information it was possible to perform the optimization of the heat transfer surfaces and to derive the best heat exchanger layout in terms of material usage. The results showed that the solution with longitudinal fins is the most efficient, with 215 kg of steel less required for the realization of the finned heat exchanger.

KEYWORDS

COMSOL Multiphysics, fin-tube heat exchanger, modelling, optimization, PCM, thermal energy storage

1 | INTRODUCTION

According to the data published by IEA in the *World Energy Outlook 2018*, energy efficiency plays a crucial role for the primary energy demand limitation. The forecasts of the energy demand are compared for different scenarios, including the new policies following the COP21 and the application of all feasible energy efficiency measures

(*Efficient World Scenario*). The increase in energy consumption by 2040, estimated at 26% with the New Policies Scenario, is around 7% if considering the implementation of all the energy efficiency measures.[1] A massive efficiency increase will be essential in the fight against greenhouse gases emissions and global warming, as reported by the IPCC report.[2]

Thermal energy storage is acknowledged as advanced energy technology and a key efficiency measure. The mismatch between supply and demand can be strongly reduced using such systems. Simultaneously, self-consumption can be enlarged due to proper management.[3-6] Latent heat thermal energy storages (LHTES) use phase change materials to store thermal energy. Usually, such materials release thermal energy from the liquid to the solid fraction. Based on this, a considerable amount of energy can be stored at a nearly constant temperature level.[7] Hence, the resulting energy density is significantly higher than conventional (sensible) systems.[8,9] The main challenge related to such applications is the considerably low thermal conductivity of PCMs. This aspect causes slow charging and discharging rates.[10]

Among the several approaches used to enhance the thermal characteristics of phase change materials, finned tube heat exchangers represent the simplest approach. They provide a high heat transfer area and their production is standardized, resulting in low manufacturing costs.[11,12] However, finned tube heat exchangers have still a significant material cost related to the high conductivity metals that are commonly used. Optimization of the heat transfer surfaces is therefore essential for limiting the system overall cost since it would allow to effectively reduce the amount of material required.[13-15] Recently studies investigated several shape and geometry of fins, from fractal tree-shaped fins to mimic the nature behaviour[16-18] up to the more classic solutions that involve radial[15] or longitudinal fins.[14] Among all these "artistic" solutions, it must be remembered that the simplicity and productivity associated with manufacturing processes are not to be overlooked.

Due to the high complexity of the involved physical mechanisms of the solid-to-liquid phase change, a purely analytical approach is not appropriate.[19-22] Analytical solutions require a significant level of simplifications, both for the heat transfer properties and for the geometrical configurations. For this reason, the design and the optimization of the LHTES were carried out by deploying a numerical model based on the Finite Element Method (FEM). This approach allows solving numerically thermal and fluid dynamic problems defined on complex geometries, as in the case of a finned tube heat exchanger. Hosseini et al (2015) showed with a numerical study, how longitudinal fins lead to less melting time and deeper penetration of heat.[14] Optimal fins were investigated numerically. All the aspects related to the numerical modelling, from the mathematical formulation of the involved physical mechanisms to the computational domain and the mesh generation, are here discussed. One of the main novelty aspects covered by the manuscript is the construction and exploitation of a numerical model for the integration of a micro-CHP generator inside a real laboratory facility using a Phase Change Material for Thermal Energy Storage (TES) purpose. Experimental tests to validate similar Finite Element Method models are poorly investigated in the literature.[7,23,24] Numerical approaches are developed to decrease the cost of experiments, however, there is a big difference considering a real case study, with a prototype and a simplified model.

The comparison between numerical and experimental results allowed us to assess the model robustness and to justify its adoption as a tool for design optimization. The validated model was finally used to study the best design of the LHTES. For the construction of the finned heat exchanger, two possible layouts were considered, with radial or longitudinal fins. In both cases, an optimization of the heat transfer surfaces is performed by investigating the relationship between the system thermal behaviour and the different HEX geometrical parameters. Based on these results, it was possible to identify the best configuration in terms of materials usage and consequently, in terms of saved costs. It was possible to save almost 215 kg of steel required for the building of the finned heat exchanger.

2 | CONTEXT AND DESIGN SPECIFICATIONS

2.1 | General framework

The envisaged LHTES is intended to be integrated with a micro-CHP system for a big office building (Energy Center, Politecnico di Torino, Turin, Italy), which provides electricity and thermal energy for both space heating and hot water. It is composed by three floors with an exposition area (925 m^2) and offices (3000 m^2), by a laboratory in the basement (327 m^2), by a laboratory closed to the main entrance (450 m^2) and by an auditorium with 150 seats (150 m^2). The building has a 47 kWp photovoltaic plant. A multipurpose geothermal heat pump (ERACS2-WQ 0802-1502, Mitsubishi Electric—Climaveneta, Italy) is installed with a power of 473 kW (heating), 442 kW (cooling) and DHW production. The maximum DHW power is fixed to 50 kW. It is planned to install in the laboratory a CHP system fed by natural gas

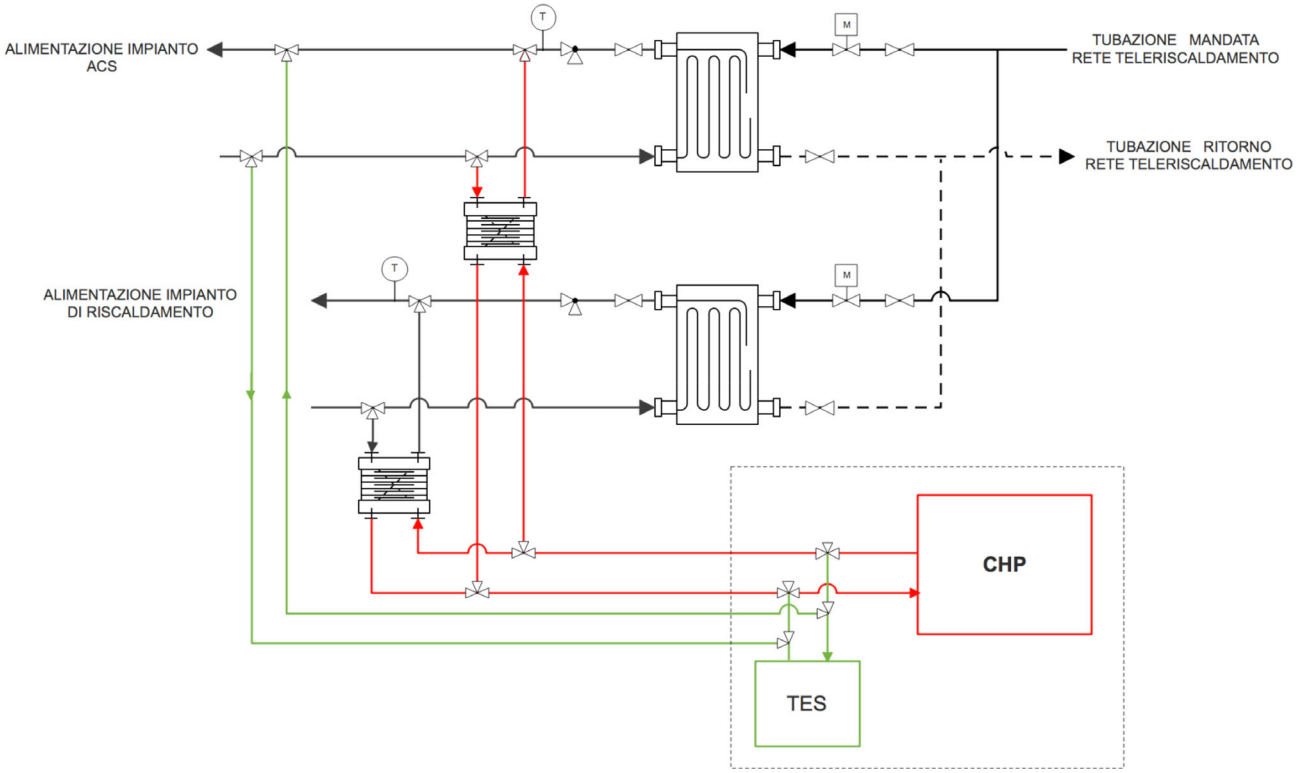

FIGURE 1 Thermal substation with CHP and heat storage system [Colour figure can be viewed at wileyonlinelibrary.com]

TABLE 1 Design specifications of the LHTES

Storage capacity (kWh)	**21**
Average thermal power (kW)	7
Discharge flowrate (L/min)	3.1
Average inlet temperature (°C)	12.4
Outlet temperature (°C)	45

to produce constantly 50 kW of thermal energy (Asja, Italy). The integration of a storage system allows the decoupling between electrical and thermal production, leading to better performances and greater flexibility (Figure 1).[3]

Known the user's technical requirements and the operating conditions for the micro-CHP, it was identified the opportunity to implement a *peak-shaving* action on the thermal load.[3] During the daily peak, the 50 kW_{th} CHP system is not able to meet all the power demand. This scenario is however limited to 3 hours per day, with a thermal demand always lower than the nominal power of the system during the remaining time. Hence, it was planned to combine the LHTES and the generation unit for the production of hot water in the peak period, which corresponds to a thermal demand of 21 kWh.

This amount of energy, representing the required storage capacity, must be delivered in a time frame of 3 hours. The LHTES must be therefore designed to fulfil an average discharge power of 7 kW. The operating conditions of the storage system are a discharge flowrate around 3.1 L/min, an inlet temperature of 12.4°C and an outlet temperature of 45°C (Table 1; Figure 2).

2.2 | Technical features

The basic layout of the LHTES corresponds to a traditional finned tube heat exchanger. Specifically, the heat transfer fluid (ie, water) passes through the heat exchanger tube bundle, while the PCM fills the shell side. The heat transfer between the storage medium and the heat transfer fluid is enhanced by the external finned surfaces embedded on the tubes. All the tests were accomplished in the start-up *i-TES* (*Turin*).

2.2.1 | Materials

The materials choice is important when dealing with latent thermal energy storage and the integration with energy production systems.

Concerning Phase Change Material, the first crucial requirement is the phase change temperature. The thermal level for the solid to liquid transition must be

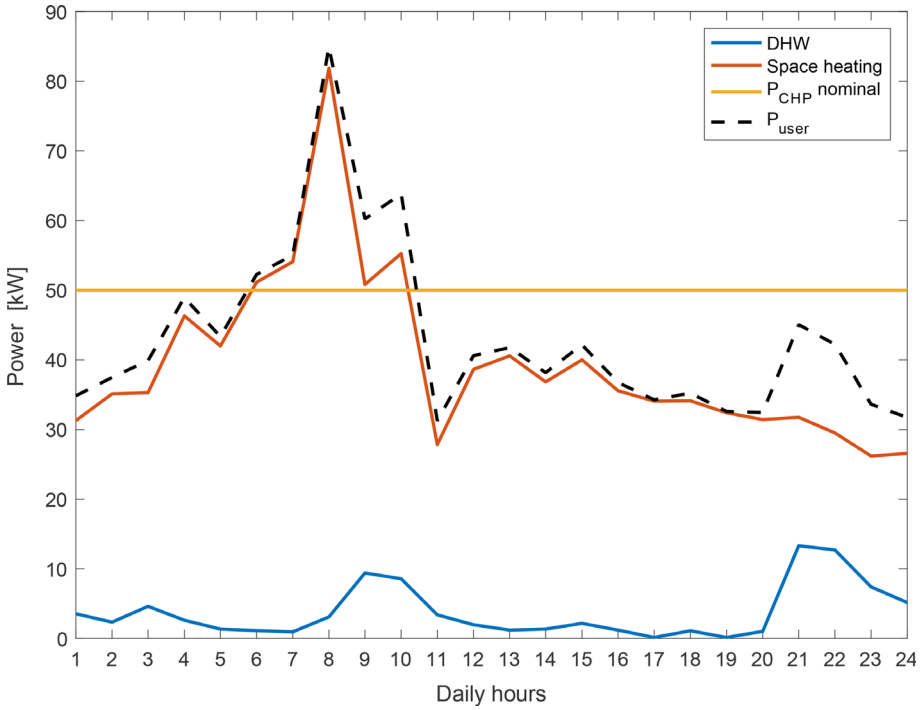

FIGURE 2 Daily trend for the demand-side thermal power [Colour figure can be viewed at wileyonlinelibrary.com]

TABLE 2 Thermophysical properties for the *CrodaTherm 60*[25]

Phase change temperature (°C)	**59.8**
Latent heat, melting (kJ/kg)	217
Density, solid (kg/m^3)	922
Density, liquid (kg/m^3)	824
Thermal conductivity, solid (W/m K)	0.29
Thermal conductivity, liquid (W/m K)	0.17
Specific heat, solid (J/kg K)	2300
Specific heat, liquid (J/kg K)	1400

coherent with the charging/discharging temperatures. For the specific case study, these values are respectively around 75°C and 45°C. Furthermore, the thermal gradient between the storage medium and the external source strongly affects the power output. The second important feature for the phase change material is then the latent heat, on which depends the storage capacity. Among the possible options, the choice fell on the *CrodaTherm 60*.[25] It is a bio-organic PCM, with a phase change temperature of 60°C, so fully compliant with the application, and great latent heat value, around 210 kJ/kg. This last feature allows to limit the amount of material required, that for a 21 kWh storage capacity is around 357 kg. The PCM selected is both chemically and physically stable, but it shows extremely low thermal conductivity values. Careful design for the heat transfer surfaces will be therefore essential to meet the required thermal performances.

Concerning instead the material used for the tube bundle, it should first of all exhibit a good thermal conductivity. Moreover, since the heat exchanger is directly in contact with the PCM, good compatibility between them is crucial. Based mainly on this second requirement, the heat transfer surfaces will be made in stainless steel (AISI 304). This material has shown during previous experiments a good interaction with the *CrodaTherm 60*. Its thermal conductivity (17 W/mK) is however of two orders of magnitude greater than the PCM one, and it is perfectly suitable for the purpose presented (Table 2).

2.2.2 | Heat transfer surfaces

For the realization of the finned tube heat exchanger, two different possible configurations of the heat transfer surfaces were considered, respectively with radial and longitudinal fins. Both of them have already been applied to LHTES, with varying results depending on the adopted PCM and the system operating conditions.[26,27] All the geometrical features (fins number, dimensions and pitch, thickness, etc.) are always limited within the feasibility range imposed by the manufacturing company (see Table 3). Pipes dimensions are instead assumed to be constant and equal to 16 mm.

The aim is to derive, for both the configurations, the optimal geometrical arrangement for the heat transfer surfaces. Optimal means obviously to meet the required thermal performance and, at the same time, to minimize

TABLE 3 Geometrical constraints for the different finned surfaces

	Radial	Longitudinal
Fin height (mm)	10 ÷ 25	4 ÷ 38
Fin thickness (kg/m^3)	1.2 ÷ 1.5	0.8 ÷ 1.5
Fins number	80 ÷ 230 (fins/m)	10 ÷ 25 (fins/tube)

the material usage for the tube bundle. Using the same criteria, it will be finally possible to establish which is the best option.

3 | NUMERICAL MODELLING

As it is well known, the unique resolving ability associated with FEM numerical models usually leads to high levels of complexity and significant computational costs. For this reason, it was necessary the development of a simplified model tailored for each specific application.

3.1 | Physics and governing equations

The overall operation of an LHTES is based on the combination of three physical mechanisms: the phase change, the heat transfer through the finned surfaces and the tube bundle and the forced convection associated with the heat transfer fluid.

3.1.1 | Heat transfer with phase change

Based on the bio-organic nature of the used PCM, the solid-to-liquid transition and its associated heat transfer were modelled by using the *apparent heat capacity method*. It belongs to the family of the *fixed domain methods,* which indirectly incorporate the latent heat contribution to the energy balance.[28] This specific feature allows moreover the use of a fixed mesh, with a great simplification of the numerical model. The method assumes that the phase change occurs on a finite thermal range and it involves the modelling of the "mushy zone," typical behaviour of organic PCMs.[10]

Since the LHTES is designed to the discharge phase, it was also decided to neglect the contribution of the convective heat transfer related to fluid motion within the liquid phase. It has been proven how, during the discharge phase, the heat transfer associated with the phase change is mainly conduction-dominated.[10,19,29] However, the model is refined considering the contribution of the forced convection of the fluid flow, as reported in the following section (Section 3.1.3).

The governing equation is based on the differential formulation of the first law of thermodynamics, which is fictitiously modified to account also for the latent heat (L). Neglecting the contribution of the fluid motion, it looks as follow:

$$\rho C_{\mathrm{p,eq}} \frac{\partial T}{\partial t} = \nabla \cdot (k \nabla T) \tag{1}$$

The specific heat of the material is replaced by its *apparent formulation* ($C_{\mathrm{p,eq}}$), which includes the latent heat distribution across the phase change temperature range (ΔT) and accounts also for the specific heat variation between the solid and the liquid phase:

$$C_{\mathrm{p,eq}} = \frac{1}{\rho}\left[\theta \rho_{\mathrm{ph1}} C_{\mathrm{p,ph1}} + (1-\theta)\rho_{\mathrm{ph2}} C_{\mathrm{p,ph2}}\right] + L\frac{d\alpha_{\mathrm{m}}}{dt} \tag{2}$$

where θ is the continuous function that describes the material state (between 0 and 1) and α_{m} is the *material fraction*, defined as

$$\alpha_{\mathrm{m}} = \frac{1}{2}\frac{(1-\theta)\rho_{\mathrm{ph2}} - \theta\rho_{\mathrm{ph1}}}{\rho} \tag{3}$$

The heat per mass unit released during the phase change is equal to the latent heat, so that:

$$\int_{T_{\mathrm{pc}}-\Delta T/2}^{T_{\mathrm{pc}}+\Delta T/2} L\frac{d\alpha_{\mathrm{m}}}{dt} = L \tag{4}$$

During the solid to liquid phase change the PCM density changes, resulting in a volume compression, together with its thermal characteristics.[25] To consider these phenomena, both an effective density and an effective thermal conductivity were also introduced:

$$\rho_{\mathrm{eff}} = \theta\rho_{\mathrm{ph1}} + (1-\theta)\rho_{\mathrm{ph2}} \tag{5}$$

$$k_{\mathrm{eff}} = \theta k_{\mathrm{ph1}} + (1-\theta)k_{\mathrm{ph2}} \tag{6}$$

3.1.2 | Heat conduction

The heat released is transferred through the finned surfaces by conduction. Its mathematical formulation is formally identical to Equation (1), where the specific heat is the one of tube bundle material.

3.1.3 | Fluid flow and forced convection

The mechanical behaviour of the heat transfer fluid is fully described by the Navier-Stokes equations for incompressible fluids[30]:

$$\nabla \cdot \boldsymbol{u} = 0 \tag{7}$$

$$\rho \frac{d\boldsymbol{u}}{dt} + \rho \boldsymbol{u} \cdot \nabla \boldsymbol{u} = -\nabla (p \cdot \boldsymbol{I}) + \mu \nabla^2 \boldsymbol{u} + \boldsymbol{F_b} \tag{8}$$

Concerning instead the convective heat transfer, the governing equation corresponds to the first law of thermodynamics in its complete form[31]:

$$\rho C_p \frac{\partial T}{\partial t} + \rho C_p u \cdot \nabla T = \nabla \cdot (k \nabla T) \tag{9}$$

To simplify the model, under the assumption of constant thermophysical properties, the problem for the heat transfer fluid was solved by adopting a *segregated approach*. Hence, the fluid dynamic part is solved first and independently from the fluid temperature profile. The derived flow field ($\boldsymbol{u}$) is then provided as input for the heat-related calculations.

3.2 | Computational domain

Based on observations concerning system geometrical features and operative conditions, it was possible to reduce the model computational domain from the whole component to a single portion of it. This allows to strongly reduce the complexity of the numerical model and its related computational cost.

The tube bundle pipes are uniformly and homogeneously arranged within the external shell. Hence, the analysis of the system thermal behaviour can be led back to that of a single *elementary module*. The computational domain was therefore always limited to one finned pipe and its attached PCM layer (see Figure 3).

Moreover, both the resulting elementary modules show specific symmetry properties, see Figure 4. For the case of radial fins, the computational domain is axially symmetric. It was so further reduced to an angular profile, moving from a 3D to a 2D model. Concerning the option with longitudinal fins, the model is still three-dimensional but with a computational domain limited to an eight of the module.

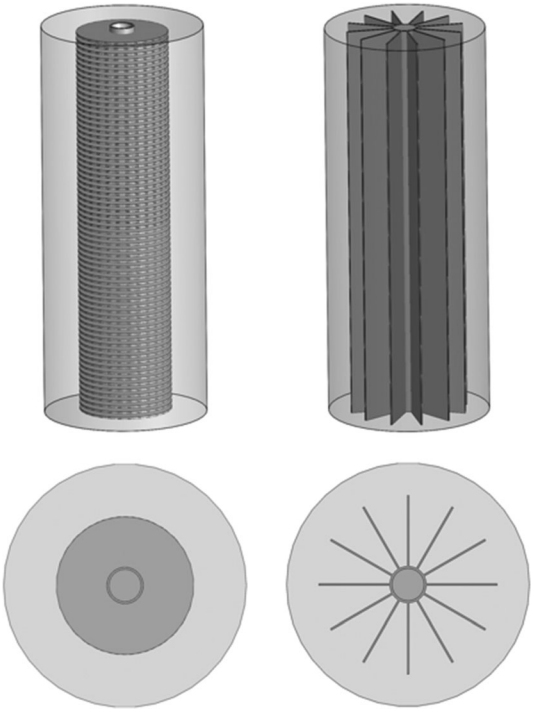

FIGURE 4 Elementary module for radial and longitudinal fins

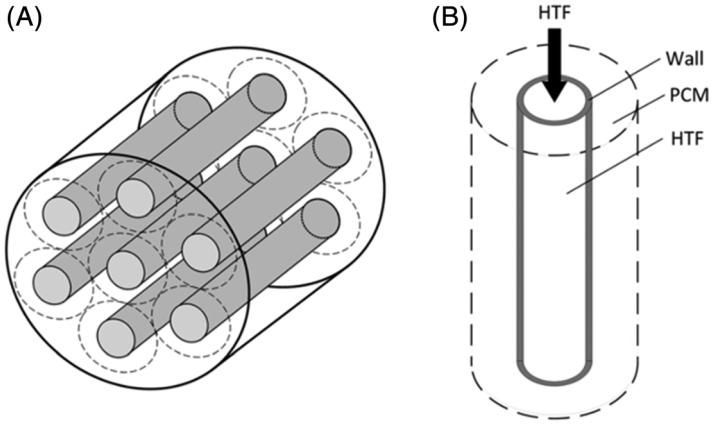

FIGURE 3 Tube bundle arrangement A, and elementary module B

3.3 | Boundary conditions

Both the differential equations for the fluid flow (7), (8) and the heat transfer (1), (9) apply only in the internal elements of the computational domain. All the conditions that describe the physical behaviour on the external boundaries need to be separately specified. For sake of simplicity, they are here reported only for the case of radial fins. Boundary conditions for the configuration with longitudinal fins are simply a three-dimensional extrapolation (Figure 5).

3.3.1 | Fluid flow

Concerning the fluid dynamic problem, the computational domain is represented by the internal area of the pipe only. The corresponding boundaries are the inlet and outlet sections ($\overline{AB}$ and $\overline{CD}$), the pipe internal surface ($\overline{BD}$) and the symmetry axis ($\overline{AC}$).

For the inlet and outlet sections the specified conditions are respectively the mass flow rate and a constant (relative) pressure:

$$-\int_{\partial\Omega} \rho(\boldsymbol{u}\cdot\boldsymbol{n}) d_{bc} dS = \dot{m}_i \tag{10}$$

$$p_0 = 0 \tag{11}$$

The interaction between the fluid and the internal pipe surface was described by applying the *no-slip condition:*

$$\boldsymbol{u} = 0 \tag{12}$$

While for the symmetry axis it was imposed the non-diffusion of the shear stresses:

$$\boldsymbol{u}\cdot\boldsymbol{n} = 0, \left(-p\boldsymbol{I} + \mu\left(\nabla\boldsymbol{u} + \nabla\boldsymbol{u}^T\right)\right)\boldsymbol{n} = 0 \tag{13}$$

3.3.2 | Heat transfer

The multiphysics heat transfer problem is defined in the whole computational domain. All the boundaries, except for the finned surfaces, need therefore a thermal specification.

The incoming fluid temperature was imposed on the inlet section, while on the outlet fully developed thermal conditions were specified:

$$T = T_{HTF,in} \tag{14}$$

$$-\boldsymbol{n}\cdot\boldsymbol{q} = 0,\ \boldsymbol{q} = -k\nabla T \tag{15}$$

Concerning instead the axis, it was sufficient to specify that no heat flow is transferred across so that the resulting temperature profile is symmetric:

$$-\boldsymbol{n}\cdot\boldsymbol{q} = 0,\ \boldsymbol{q} = -k\nabla T \tag{16}$$

All the other boundaries, including the external PCM surface because of the symmetry condition, are finally adiabatic. From the mathematical point of view, this is formally identical to what already specified for the axis.

3.4 | Mesh generation

The procedure of domain discretization, needed to address the problem numerically, is reflected by the mesh generation. It has direct leverage on the simulation model, affecting both the convergence and the solution accuracy.[32,33] For this reason, a careful grid independence analysis accounting for all the key parameters was always performed.

3.4.1 | Radial fins

The 2D axisymmetric computational domain was discretized using a polygonal mesh with triangular

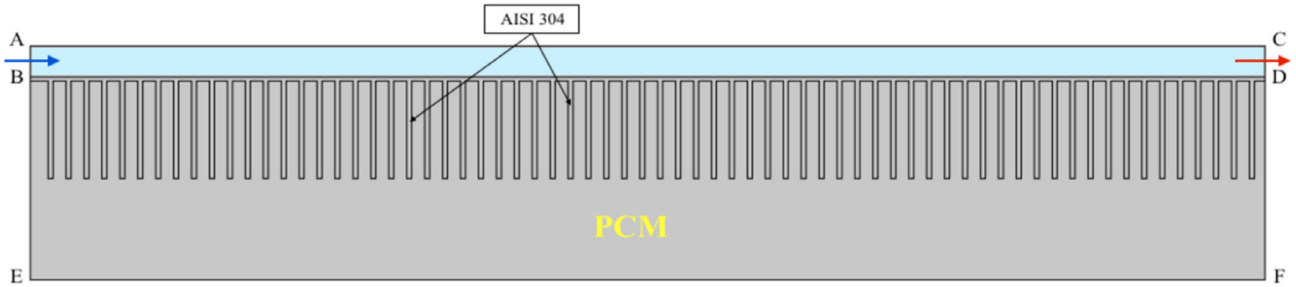

FIGURE 5 Computational domains for the 2D axial symmetric model [Colour figure can be viewed at wileyonlinelibrary.com]

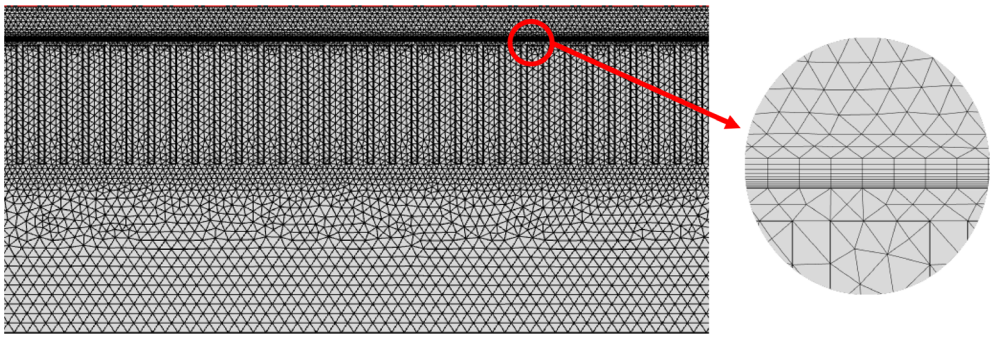

FIGURE 6 Structured polygonal mesh for the case of radian fins [Colour figure can be viewed at wileyonlinelibrary.com]

elements. The core mesh was customized to be more refined closer to the solid-to-liquid interface, where the higher thermo-fluid dynamic gradients appear. Moreover, the pipe internal boundary was equipped with a prismatic layer, essential to properly resolve the thermal problem.[33]

Following the grid independence analysis (see the Supplementary Material), the adopted mesh presents on the whole 143 000 triangular elements and a 10-element prismatic layer (Figure 6).

3.4.2 | Longitudinal fins

The same general comments made on the mesh structure apply also for the case of longitudinal fins. The only difference is related to the three-dimensionality of the model.

Given the symmetry features of the computational domain, it was decided to use an *extruded mesh*. It is made up of hexahedral elements, obtained by extruding a triangular mesh defined on the module frontal surface. This solution allows to strongly reduce the number of elements and it is, of course, compliant with the physics of the problem, which is characterized by weak thermal gradients in the axial direction.[34] After performing the grid independence analysis (see the Supplementary Material), it was established a 3D mesh with 71 000 hexahedral elements, a maximum element axial dimension of 10 mm and a 10-element prismatic layer (Figure 7).

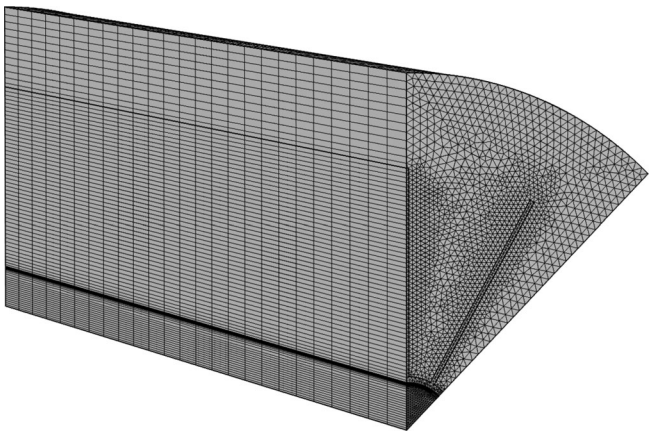

FIGURE 7 Structured 3D hexagonal mesh for the case of longitudinal fins

3.5 | Experimental test and model validation

To verify all the assumptions and assess their accuracy, the developed numerical model was submitted to a validation procedure. To do this, a small LHTES prototype in the form of a tube-in-tube finned heat exchanger was built and tested in the *i-TES* laboratories (Figure 8).

The experimental set-up was designed to allow a discharge with constant HTF inlet temperature and mass flow rate. During the discharge phase, the cold fluid coming from the water network flows directly through the LHTES prototype. To perform the charge of the storage unit the water is recirculated in a closed-loop by using a diaphragm pump (Shurflo 2095-204-112, Pentair). The amount of thermal energy released by the HTF through the heat exchanger and absorbed by the PCM is supplemented by an external thermostat (Velp scientifica, Italy). The device is equipped with a proper control system, which allows to keep the fluid inlet temperature almost constant. Since the numerical model is intended to predict the thermal performances of the system, the tests focused on measuring the heat transfer rate (Q_{HTF}). Temperature sensors (K-type thermocouples, DollaTek, Hongkong Yingli International trading co limited, HK) was thus installed at the inlet and the outlet of the storage unit to measure the HTF temperature drop.

$$Q_{HTF} = \dot{m}_{HTF} \cdot C_p \cdot (T_{HTF,out} - T_{HTF,in}) \quad (17)$$

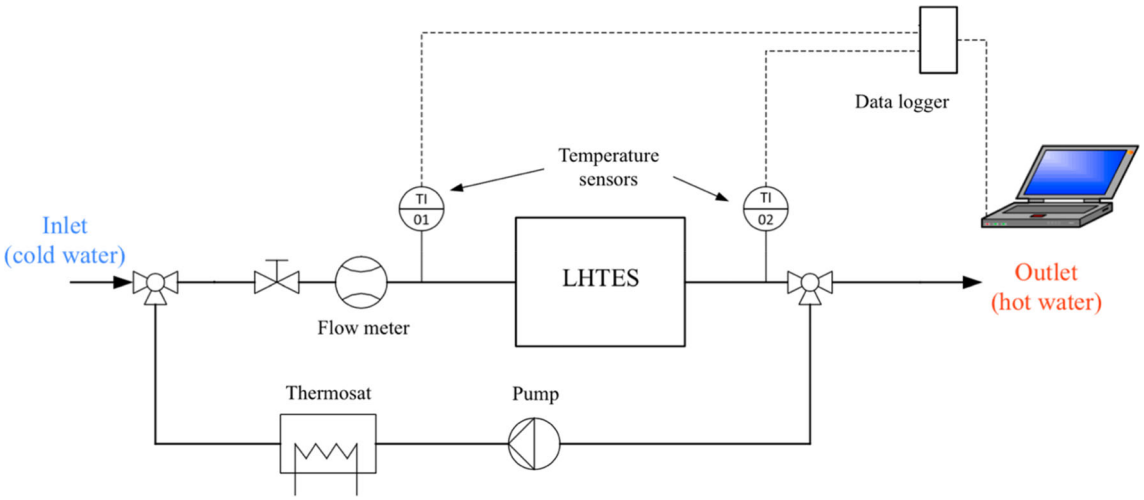

FIGURE 8 Schematic of the experimental set-up [Colour figure can be viewed at wileyonlinelibrary.com]

4 | RESULTS AND DISCUSSIONS

As already introduced, the LHTES thermal performances are strongly affected by the heat exchanger design and its heat surfaces geometrical features. To assess the connection between performances and design parameters and to derive the optimal layout, the dynamic thermal behaviour of the system was simulated by applying the presented FEM numerical model.

4.1 | Problem of optimization

4.1.1 | Design variables

The finned heat exchanger layout may depend on several geometrical parameters, which can have a greater or lesser impact on both its thermal behaviour and material usage. Among all of them, only three parameters were identified as leading variables: the cross-sectional pitch of the tube bundle (*p*), the fin dimension *(H)* and fins specific number *(n)*.

The overall heat transfer area varies as a consequence with the parameters reported above. This affects the system thermal performances. However, their associated surface variations are not to the same extent. The impact in terms of material usage of the tube bundle pitch is always considerably more crucial (see Figure 9).

4.1.2 | Optimization criteria

In short, the tube bundle material amount represents the objective function (to be minimized) for the optimization problem, while the pitch, the fin dimension and the fins number are the three free variables. The optimization is of course constrained, by both the fins geometrical limits and the required thermal performances.

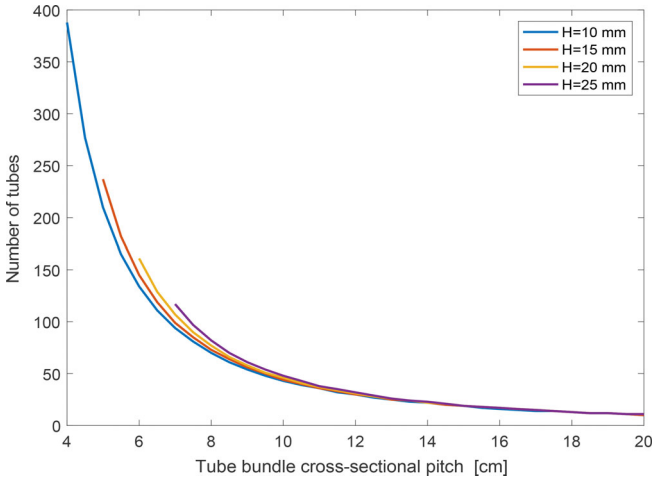

FIGURE 9 Influence of *p* and *H* on the required material usage (radial fins, n = 230 fins/m) [Colour figure can be viewed at wileyonlinelibrary.com]

The approach used to derive the optimal combination of the geometrical parameters is the following:

1. Based on its strong impact on the amount of material, it was first assessed the minimum number of tubes required for the heat exchanger by acting on the cross-sectional pitch (*p*) only. In this first stage, all the other variables are kept constant and equal to their maximum allowed value. The minimum acceptable number of pipes is, therefore, that which corresponds to an average thermal power greater, or equal, than the specified design value (7 kW).

2. The amount of material was then minimized acting on the fins geometrical features. This was achieved by identifying, case by case, which is the geometrical parameter that has the strongest effect on the system thermal behaviour. The leading variable is, of course, the one that, in response to the same material reduction, shows the greatest thermal output reduction. Hence, it was kept constant and equal to its maximum value, while the other parameter was finally adjusted until reaching the design thermal power.

The same procedure was, of course, applied identically for both the fins arrangements.

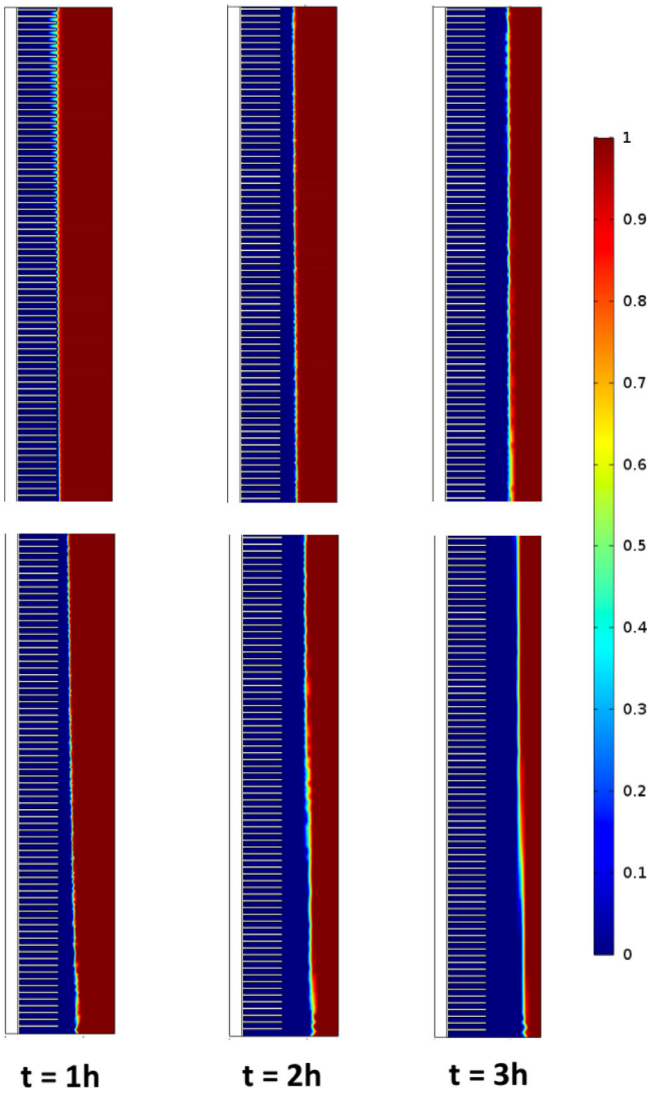

FIGURE 10 Solid–liquid interface progression during the discharge phase, at the end of the tube (top part) and the initial portion of the tube (bottom part)—($P = 14$ cm, $H = 25$ mm, $n = 230$ fins/m)—(1 is the liquid fraction while 0 is the solid fraction) [Colour figure can be viewed at wileyonlinelibrary.com]

4.2 | Radial fins

Starting from an initial value for the cross-sectional pitch (p_0) of 14 cm, the predicted heat transfer rate was around 4.47 kW, well below the design target (7 kW). In this first stage the fins geometrical parameters are equal to their maximum allowable values, namely $H = 25$ mm and $n = 230$ fins/m (Figure 10).

The cross-sectional pitch was thus gradually reduced until finding the minimum required number for the tube bundle pipes, which showed up to be 48 ($P = 10$ cm). The average power output is in this case of 7.2 kW. The improvement of the thermal performances, from 4.47 to 7 kW is paid with a 109% increase of the required material amount for the heat exchanger, which raises from 199 kg up to 415 kg. The relationship between the thermal performances and material usage is implemented in the model and it is a function of transverse pitch, fixing the optimal value for the fins height and the number of fins, see Figure 11.

Since the corresponding thermal power is slightly higher than the design value, the heat transfer area can be reduced acting on the fins parameters. To assess the leading variable, the system thermal behaviour was compared for two different configurations with the same 12.5% steel reduction (−59 kg). The first configuration presents a parameter H reduced from 25 to 23 mm, while in the second one it is the number of fins that decreases from 230 to 195 fins/m.

The outcomes showed that, for the radial configuration, it is the fin height (H) to have the strongest impact on the system thermal performances. This outcome is supported also by other similar studies.[13] Yang et al (2017) investigated the role of annular fins and the fin

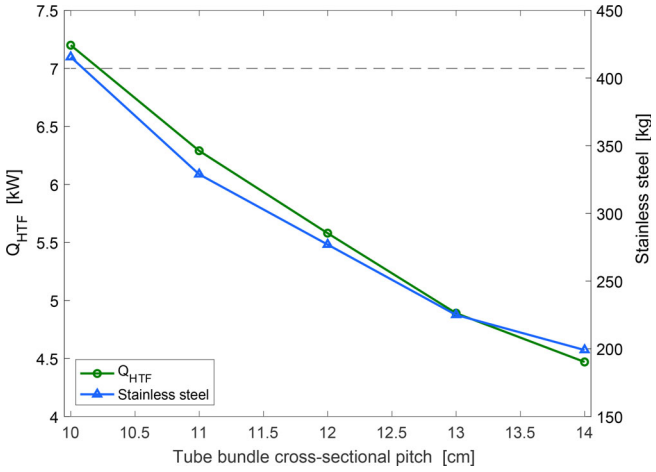

FIGURE 11 Dependence of thermal performances and material usage on the cross-sectional pitch ($H = 25$ mm, $n = 230$ fins/m) [Colour figure can be viewed at wileyonlinelibrary.com]

height is one of the main parameters that influence the heat transfer. This is due to the local convection in the PCM phase that strongly promotes the interface evolution accelerating the thermal transmission, as reported elsewhere.[27]

Therefore, the fins density on the pipes outer surfaces was gradually decreased until 185 fins/m, which corresponds to a 7.06 kW average thermal power. While the system performances showed a reduction of only 1.9%, the related material usage dropped by 19% (−76 kg), see Figure 12.

4.3 | Longitudinal fins

In this case, the starting point for the analysis was a configuration with a cross-sectional pitch (p_o) of 12 cm and fins with the following geometry: 35 mm (H) and 12 fins/pipe (n). The associated thermal performance obtained from the model is around 5.5 kW. This value is not satisfactory considering the starting target around 7 kW (Figure 13).

It was applied the same procedure described above. The first results achieved from the model is a minimum number of pipes, which corresponds to a P-value of 9 cm. The thermal output grows up to 7.44 kW, with a consequent 45% increase in the material amount required for the tube bundle (Figure 14).

The assessment of the leading variable was performed by comparing two different configurations with a 30% material reduction, one obtained decreasing the fin height to 25 mm and the other reducing the fins number to the value of 8 fins/tube. The results showed that this time, it is the number of fins that produces the strongest effect on the system thermal performances. For the case of $H = 25$ mm the average thermal power falls in fact to 6.9 kW, while with n = 8 fins/tube it is around to 7.2 kW.

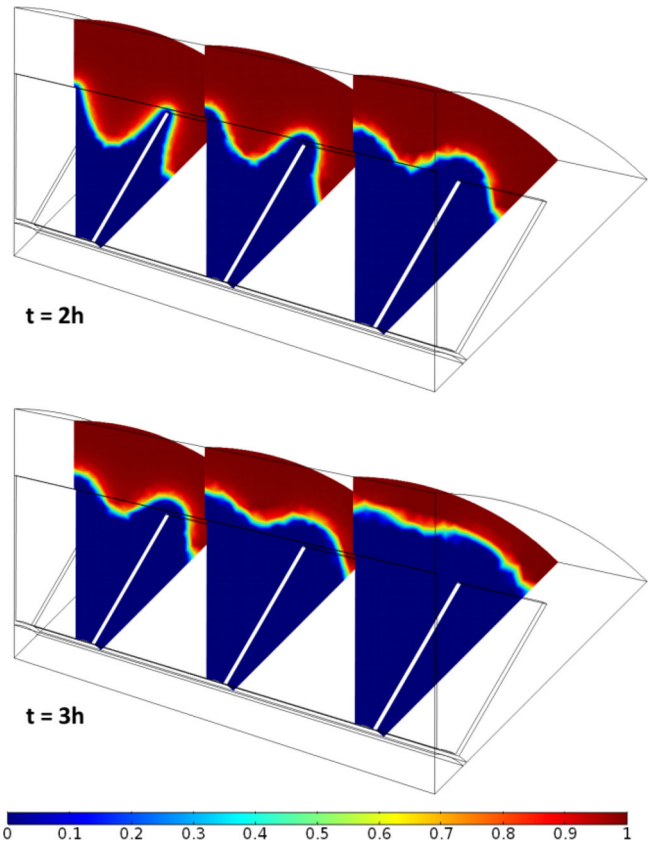

FIGURE 13 Solid–liquid interface progression during the discharge phase ($P = 12$ cm, $H = 35$ mm, $n = 12$ fins/tube) (1 is the liquid fraction while 0 is the solid fraction) [Colour figure can be viewed at wileyonlinelibrary.com]

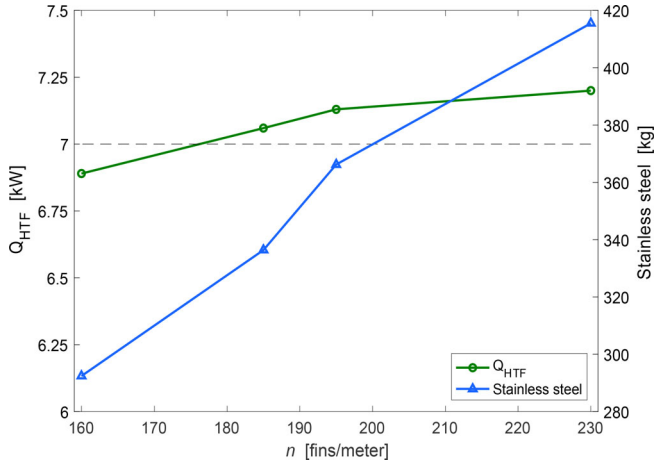

FIGURE 12 Dependence of thermal performances and material usage on the fins density ($P = 10$ cm, $H = 25$ mm) [Colour figure can be viewed at wileyonlinelibrary.com]

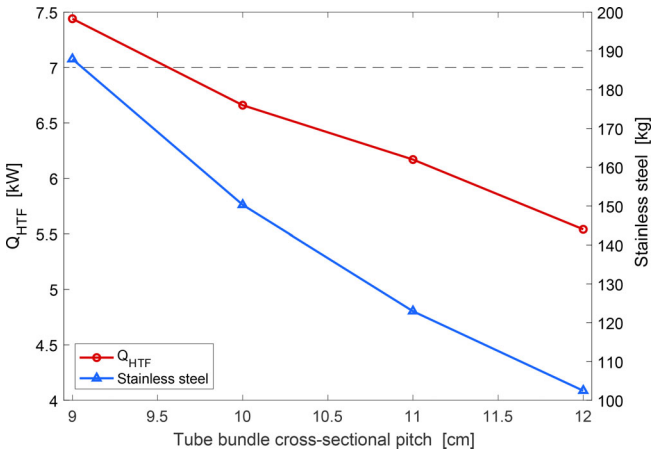

FIGURE 14 Dependence of thermal performances and material usage on the cross-sectional pitch ($H = 35$ mm, $n = 12$ fins/tube) [Colour figure can be viewed at wileyonlinelibrary.com]

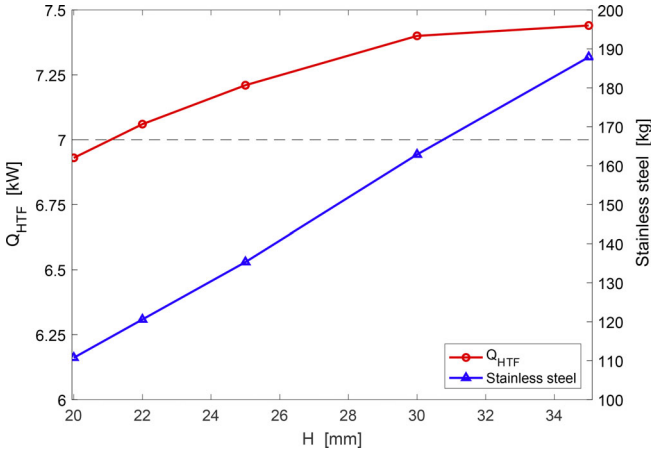

FIGURE 15 Dependence of thermal performances and material usage on the fins density ($P = 9$ cm, $n = 12$ fins/tube) [Colour figure can be viewed at wileyonlinelibrary.com]

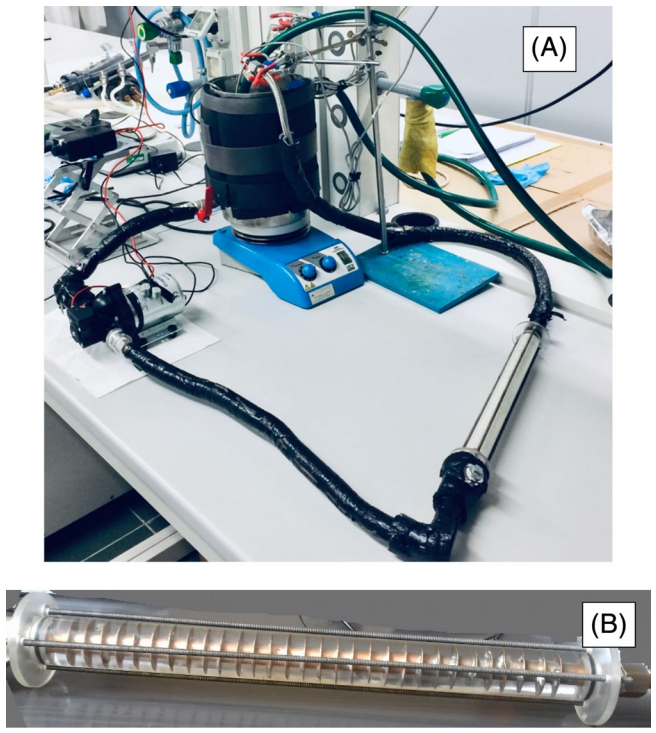

FIGURE 16 LHTES prototype and experimental set-up: A, general view; B, detail of the heat exchanger with radial fins [Colour figure can be viewed at wileyonlinelibrary.com]

Hosseini et al (2015) showed how the fins height, fixing the number of fins, affect the thermal performance, but at the expense of the cost of constructing the exchanger.[14] However, acting on the number of fins interesting results are achieved by improving the heat transfer. In fact, the solidification and heat transfer front improves, more considering the number of fins compared to their height. This is due to the establishment of local convection

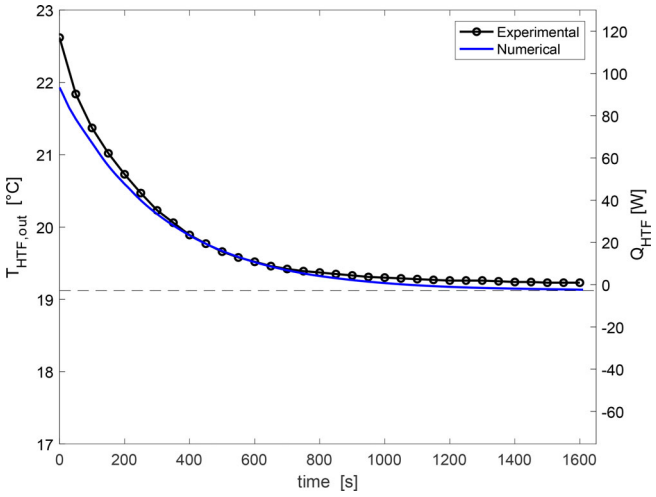

FIGURE 17 Comparison between numerical and experimental results [Colour figure can be viewed at wileyonlinelibrary.com]

phenomena, which allow a better thermal exchange. Similar behaviour was shown from Rahimi et al (2014),[15] where the solidification process is more affected by using fins rather than by their height.

Therefore, to derive the optimal arrangement, the fins height (H) was reduced to 22 mm. The corresponding average thermal power is 7.05 kW, with an associated material reduction of 67 kg (Figure 15).

4.4 | Validation of the model

Starting from a completely charged state with liquid PCM, the small LHTES was subjected to an inlet fluid temperature of 19°C and a water flow rate of 0.51 L/min. The experimental test bench is depicted in the following figure. From the comparison between the experimental results and the numerical prediction was then possible to evaluate the model robustness (Figure 16).

The achieved results, given in Figure 17, proved that the simplified model was able to predict properly the thermal behaviour of the system. The discharged heat power trend derived from the simulations reflects loyally the real measured power output, with a maximum error of 3% and an average value of 0.48%.

5 | CONCLUSION

A simplified FEM numerical model was developed and validated to perform the design and the optimization of a 7.2 kW thermal latent heat energy storage. The introduced simplifications proved to be compliant with all the

TABLE 4 Comparison between the optimal arrangements of the different layouts

	Radial	Longitudinal
Tube bundle pitch (cm)	10	9
Number of pipes (−)	48	55
Average thermal power (kW)	7.06	7.05
Heat transfer surface (m^2)	70.88	36.85
Stainless steel (kg)	336.4	121.0

relevant physical mechanisms, allowed to achieve a reliable and easy-to-use computational tool. This confirms how numerical modelling represents an effective alternative in the complex design of the LHTESs.

For the layout of the heat transfer surfaces two different arrangements were considered, respectively with radial and longitudinal fins. By exploiting the numerical model, an optimization procedure for the finned tube heat exchanger was carried out. In each case, it was proved the possibility to achieve a system able to meet the design requirements, for both the storage capacity and the heat transfer rate. Moreover, each of them presents an optimal combination of the HEX geometrical parameters that allowed the minimization of the required material usage.

However, even though the average thermal output is the same, the two resulting designs showed different technical features (see Table 4). This confirms the great importance, for an LHTES, of the adopted heat transfer enhancement technique. The layout with longitudinal fins is in this case undoubtedly the most efficient option. The resulting heat transfer surface is 64% smaller than the competing option, with only 121 kg of stainless steel required for the finned tube heat exchanger.

This result will allow to choose the best system design and, therefore, to strongly reduce its manufacturing cost.

NOMENCLATURE

DHW	domestic hot water
FEM	finite element method
HEX	heat exchanger
HTF	heat transfer fluid
IPCC	intergovernmental panel on climate change
LHTES	latent heat thermal energy storages
micro-CHP generator	micro combined heat and power generator
PCMs	phase change materials
TES	thermal energy storages

UNITS OF MEASURE

T	temperature, K
ρ	density, kg/m^3
C_p	specific heat, J/(kg K)
k	thermal conductivity, W/(m K)
ϑ	PCM material fraction, −
ρ_{ph1}	PCM density in the solid phase, kg/m^3
ρ_{ph2}	PCM density in the liquid phase, kg/m^3
ρ_{eff}	PCM effective density, kg/m^3
k_{ph1}	PCM thermal conductivity in the solid phase, W/(m K)
k_{ph2}	PCM thermal conductivity in the liquid phase, W/(m K)
k_{eff}	PCM effective thermal conductivity, W/(m K)
$C_{p,ph1}$	PCM specific heat in the solid phase, J/(kg K)
$C_{p,ph2}$	PCM specific heat in the liquid phase, J/(kg K)
$C_{p,eq}$	PCM apparent heat capacity, J/(kg K)
L	PCM latent heat, J/kg
α_m	PCM material fraction, −
T_{pc}	phase change temperature, °C
ΔT	phase change temperature range, °C
U	heat transfer fluid velocity, m/s
p	heat transfer fluid pressure, Pa
μ	heat transfer fluid dynamic viscosity, Pa·s
F_b	heat transfer fluid body force, N/m^3
m_i	mass flow rate for a single pipe of the bundle, kg/s
$T_{HTF,in}$	heat transfer fluid inlet temperature, °C
$T_{HTF,out}$	heat transfer fluid outlet temperature, °C
$\dot{m}_{HTF}$	heat transfer fluid mass flow rate, kg/s
$Q_{HTF,out}$	exchanged thermal power, W

ORCID

Maurizio Bressan https://orcid.org/0000-0002-0652-2614
Davide Papurello https://orcid.org/0000-0003-1455-8964

REFERENCES

1. OECD/IEA, 2018 World energy outlook: executive summary, (2018) 11.
2. IPCC-Report Global warming of 1.5°C, 2018. https://www.ipcc.ch/sr15/download/ (accessed August 15, 2020).
3. Dincer I, Rosen M. *Thermal Energy Storage: Systems and Applications*. 2nd ed. West Sussex, England: Wiley; 2002. https://www.wiley.com/en-us/Thermal+Energy+Storage%3A+Systems+and+Applications%2C+2nd+Edition-p-9780470747063 (accessed August 15, 2020).
4. Pagkalos C, Dogkas G, Koukou MK, Konstantaras J, Lymperis K, Gr M. Vrachopoulos, evaluation of water and paraffin PCM as storage media for use in thermal energy storage applications: a numerical approach. *Int J Thermofluids*. 2020;1–2:100006. https://doi.org/10.1016/j.ijft.2019.100006.

5. Liang H, Niu J, Gan Y. Performance optimization for shell-and-tube PCM thermal energy storage. *J Energy Storage*. 2020; 30:101421. https://doi.org/10.1016/j.est.2020.101421.
6. Dadollahi M, Mehrpooya M. Modeling and investigation of high temperature phase change materials (PCM) in different storage tank configurations. *J Clean Prod*. 2017;161:831-839. https://doi.org/10.1016/j.jclepro.2017.05.171.
7. Faraj K, Khaled M, Faraj J, Hachem F, Castelain C. A review on phase change materials for thermal energy storage in buildings: heating and hybrid applications. *J Energy Storage*. 2021; 33:101913. https://doi.org/10.1016/j.est.2020.101913.
8. Sarbu I, Sebarchievici C. A comprehensive review of thermal energy storage. *Sustainability*. 2018;10:191. https://doi.org/10.3390/su10010191.
9. Liu M, Riahi S, Jacob R, Belusko M, Bruno F. Design of sensible and latent heat thermal energy storage systems for concentrated solar power plants: thermal performance analysis. *Renew Energy*. 2020;151:1286-1297. https://doi.org/10.1016/j.renene.2019.11.115.
10. Fleischer AS. Fundamental thermal analysis. In: Fleischer AS, ed. *Therm. Energy Storage Using Phase Change Mater. Fundam. Appl*. Cham, Switzerland: Springer International Publishing; 2015:75-85. https://doi.org/10.1007/978-3-319-20922-7_5.
11. Agyenim F, Hewitt N, Eames P, Smyth M. A review of materials, heat transfer and phase change problem formulation for latent heat thermal energy storage systems (LHTESS). *Renew Sustain Energy Rev*. 2010;14:615-628. https://doi.org/10.1016/j.rser.2009.10.015.
12. Mohamed SA, Al-Sulaiman FA, Ibrahim NI, et al. A review on current status and challenges of inorganic phase change materials for thermal energy storage systems. *Renew Sustain Energy Rev*. 2017;70:1072-1089. https://doi.org/10.1016/j.rser.2016.12.012.
13. Yang X, Lu Z, Bai Q, Zhang Q, Jin L, Yan J. Thermal performance of a shell-and-tube latent heat thermal energy storage unit: role of annular fins. *Appl Energy*. 2017;202:558-570. https://doi.org/10.1016/j.apenergy.2017.05.007.
14. Hosseini MJ, Ranjbar AA, Rahimi M, Bahrampoury R. Experimental and numerical evaluation of longitudinally finned latent heat thermal storage systems. *Energy Build*. 2015;99:263-272. https://doi.org/10.1016/j.enbuild.2015.04.045.
15. Rahimi M, Ranjbar AA, Ganji DD, Sedighi K, Hosseini MJ, Bahrampoury R. Analysis of geometrical and operational parameters of PCM in a fin and tube heat exchanger. *Int Commun Heat Mass Transfer*. 2014;53:109-115. https://doi.org/10.1016/j.icheatmasstransfer.2014.02.025.
16. Wu S, Huang Y, Zhang C, Chen Y. Role of tree-shaped fins in charging performance of a latent heat storage unit. *Int J Energy Res*. 2020;44:4800-4811. https://doi.org/10.1002/er.5268.
17. Zhang C, Li J, Chen Y. Improving the energy discharging performance of a latent heat storage (LHS) unit using fractal-tree-shaped fins. *Appl Energy*. 2020;259:114102. https://doi.org/10.1016/j.apenergy.2019.114102.
18. Sarani I, Payan S, Nada SA, Payan A. Numerical investigation of an innovative discontinuous distribution of fins for solidification rate enhancement in PCM with and without nanoparticles. *Appl Therm Eng*. 2020;176:115017. https://doi.org/10.1016/j.applthermaleng.2020.115017.
19. Cabeza LF. *Advances in Thermal Energy Storage Systems*, Methods and Applications. London, England: Elsevier, 2015. https://doi.org/10.1016/C2013-0-16453-7.
20. Zalba B, Marin JM, Cabeza LF, Mehling H. Review on thermal energy storage with phase change: materials, heat transfer analysis and applications. *Appl Therm Eng*. 2003;23:251-283. https://doi.org/10.1016/S1359-4311(02)00192-8.
21. Khan Z, Khan Z, Ghafoor A. A review of performance enhancement of PCM based latent heat storage system within the context of materials, thermal stability and compatibility. *Energy Convers Manage*. 2016;115:132-158. https://doi.org/10.1016/j.enconman.2016.02.045.
22. Al-abidi AA, Bin Mat S, Sopian K, Sulaiman MY, Mohammed AT. CFD applications for latent heat thermal energy storage: a review. *Renew Sustain Energy Rev*. 2013;20:353-363. https://doi.org/10.1016/j.rser.2012.11.079.
23. Devaux P, Farid MM. Benefits of PCM underfloor heating with PCM wallboards for space heating in winter. *Appl Energy*. 2017;191:593-602. https://doi.org/10.1016/j.apenergy.2017.01.060.
24. Vanaga R, Blumberga A, Freimanis R, Mols T, Blumberga D. Solar facade module for nearly zero energy building. *Energy*. 2018;157:1025-1034. https://doi.org/10.1016/j.energy.2018.04.167.
25. CrodaTherm 60, Croda phase change materials (n.d.). https://www.crodatherm.com/en-gb/products-and-applications/product-finder/product/1366/CrodaTherm_1_60 (accessed August 17, 2020).
26. Rozenfeld A, Kozak Y, Rozenfeld T, Ziskind G. Experimental demonstration, modeling and analysis of a novel latent-heat thermal energy storage unit with a helical fin. *Int J Heat Mass Transfer*. 2017;110:692-709. https://doi.org/10.1016/j.ijheatmasstransfer.2017.03.020.
27. Sciacovelli A, Gagliardi F, Verda V. Maximization of performance of a PCM latent heat storage system with innovative fins. *Appl Energy*. 2015;137:707-715. https://doi.org/10.1016/j.apenergy.2014.07.015.
28. A. Machniewicz, D. Heim, Modelling of latent heat storage in PCM modified components, (n.d.) 7.
29. Mehling H, Cabeza LF. Design of latent heat storages. In: Mehling H, Cabeza LF, eds. *Heat Cold Storage PCM Date Introd. Basics Appl*. Berlin, Heidelberg: Springer; 2008:137-179. https://doi.org/10.1007/978-3-540-68557-9_5.
30. Munson BR, Okiishi TH, Huebsch WW, Rothmayer AP. *Fundamentals of Fluid Mechanics 7th Edition, 2013—Munson*. 7th ed. Dallas, TX: John Wiley & Sons, Inc.; 2013. http://www.pdfdrive.com/fundamentals-of-fluid-mechanics-7th-edition-2013-munson-d144739981.html (accessed August 17, 2020).
31. Incropera FP, Incropera FP, eds. *Fundamentals of Heat and Mass Transfer*. 6th ed. Hoboken, NJ: John Wiley; 2007.
32. Versteeg HK, Malalasekera W. *An Introduction to Computational Fluid Dynamics: the Finite Volume Method*. Glasgow, UK: Pearson Education; 2007.
33. Ferziger JH, Perić M. Finite volume methods. In: Ferziger JH, Perić M, eds. *Comput. Methods Fluid Dyn*. Berlin, Heidelberg: Springer; 2002:71-89. https://doi.org/10.1007/978-3-642-56026-2_4.
34. Agyenim F, Eames P, Smyth M. A comparison of heat transfer enhancement in a medium temperature thermal energy storage

heat exchanger using fins. *Sol Energy*. 2009;83:1509-1520. https://doi.org/10.1016/j.solener.2009.04.007.

SUPPORTING INFORMATION

Additional supporting information may be found online in the Supporting Information section at the end of this article.

How to cite this article: Triscari G, Santovito M, Bressan M, Papurello D. Experimental and model validation of a phase change material heat exchanger integrated into a real building. *Int J Energy Res*. 2021;1-15. https://doi.org/10.1002/er.7037